Developing Optical Sensors with Application of Cancer Detection by Elastic Light Scattering Spectroscopy

May Fadheel Estephan, Richard Perks

Abstract—Cancer is a serious health concern that affects millions of people worldwide. Early detection and treatment are essential for improving patient outcomes. However, current methods for cancer detection have limitations, such as low sensitivity and specificity. The aim of this study was to develop an optical sensor for cancer detection using elastic light scattering spectroscopy (ELSS). ELSS is a non-invasive optical technique that can be used to characterize the size and concentration of particles in a solution. An optical probe was fabricated with a 100-μm-diameter core and a 132-μm centre-to-centre separation. The probe was used to measure the ELSS spectra of polystyrene spheres with diameters of 2 μm, 0.8 μm, and 0.413 μm. The spectra were then analysed to determine the size and concentration of the spheres. The results showed that the optical probe was able to differentiate between the three different sizes of polystyrene spheres. The probe was also able to detect the presence of polystyrene spheres in suspension concentrations as low as 0.01%. The results of this study demonstrate the potential of ELSS for cancer detection. ELSS is a non-invasive technique that can be used to characterize the size and concentration of cells in a tissue sample. This information can be used to identify cancer cells and assess the stage of the disease. The data for this study were collected by measuring the ELSS spectra of polystyrene spheres with different diameters. The spectra were collected using a spectrometer and a computer. The ELSS spectra were analysed using a software program to determine the size and concentration of the spheres. The software program used a mathematical algorithm to fit the spectra to a theoretical model. The question addressed by this study was whether ELSS could be used to detect cancer cells. The results of the study showed that ELSS could be used to differentiate between different sizes of cells, suggesting that it could be used to detect cancer cells. The findings of this research show the utility of ELSS in the early identification of cancer. ELSS is a non-invasive method for characterizing the number and size of cells in a tissue sample. To determine cancer cells and determine the disease's stage, this information can be employed. Further research is needed to evaluate the clinical performance of ELSS for cancer detection.

Keywords—Elastic Light Scattering Spectroscopy, Polystyrene spheres in suspension, optical probe, fibre optics.

I. INTRODUCTION

DESPITE significant progress in cancer research, the disease remains a major health concern. In certain cases of cancer, a biopsy has allowed for a precise diagnosis and subsequent treatment strategy. However, this is typically time-consuming and costly because it requires many sampling points and is generally insensitive. To improve the diagnosis of tumours originating from a variety of sources, optical spectroscopy has been utilized [1]-[3]. This method has been shown to be the most effective for distinguishing between normal and malignant tissues by describing the alterations in the characteristics of tissue structure, cell shape, and metabolic composition that characterize cancer. Characterization of tissues is made possible with this method by means of optical spectral measurements. ELSS, diffuse reflectance spectroscopy (DRS), fluorescence spectroscopy (FS), and Raman spectroscopy (RS) are various aspects of optical spectroscopy that have been employed. ELSS was chosen as the focus of our investigation for a variety of reasons. To begin, the efficiency and sensitivity of ELSS is higher than that of other optical approaches (FS and RS) because ELSS signals are stronger. Second, due to the magnitude of the optical signal, elastic scattering has the potential to be the fastest and most cost-effective among the numerous optical detection systems [4]. By detecting the white light that is scattered back from tissues, ELSS can detect light that has been reflected or scattered off of human tissue using optical fibres of a certain diameter and geometry. The edges of cells and subcellular structures are sites of this scattering mechanism [5]. Back reflection spectroscopy is essential for detection because it can determine the optical characteristics of diseased tissue [6]. ELSS is an optical method that could one day be used to conduct a non-invasive biopsy. Without modifying the wavelength, ELSS involves light's penetration into tissue and subsequent backscatter. Due to differences in cellular morphology, the spectrum of backscattering varies. For instance, as the size or number of mitochondria increases, the scattering characteristics will change (Fig. 1). Additionally, the ELSS signal makes it simple to detect the absorption properties (the tissue's metabolic function) [7]. Dispersion arises because of variations in cellular and subcellular densities [8]. Those parts of a cell known as "scattering centres" have their unique properties encoded in the scattering event. Pathological scattering is characterized by alterations of the texture, thickness, and architecture of the epithelial surface, altered epithelial cell orientations, cell crowding, increased distance from the subepithelial collagen layer, enlarged and hyperchromic nuclei, increased concentration of metabolic organelles, and the presence of

May Fadheel Estephan is with Department of Physiology and Medical Physics, College of Medicine, Al-Nahrain University, Al-Kadhimyia - Str. 60 Baghdad, Iraq (e-mail: mayestephan@gmail.com).

Richard Perks is with School of Engineering, Cardiff University, CF24 3AA Cardiff, U.K.

World Academy of Science, Engineering and Technology
International Journal of Biomedical and Biological Engineering
Vol:18, No:5, 2024

abnormal protein particles or packages [9]. As a result, a straightforward mathematical model depicting the probe's two identical fibre optic wires has been developed. The scattered intensity of light as it is absorbed by an adjacent fibre is a function of the diameter of the fibres involved, their relative distance apart, and the scattering angle. For the purpose of detecting an application of cancer, an optical probe has been fabricated and employed by using an artificial tissue.
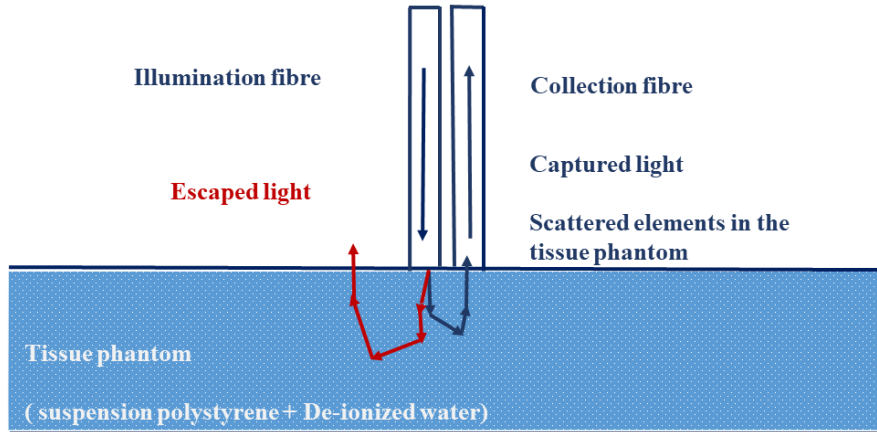

Fig. 1 Schematic set up of the ELSS

A. Biological Tissues' Optical Properties

In a new era of contemporary medicine, the progress of optical procedures relies heavily on the identification of the optical properties of diverse biological tissues [10]. The diagnostic utility of the light that emerges from the fibre after penetrating and probing the tissue components is enhanced [11], [12]. However, the capability to penetrate and deposit energy via tissue is determined by the therapeutic uses [13], [14]. The optical characteristic of tissue is explained by the scattering coefficient (μ_s), absorption coefficient (μ_a), scattering function P (θ, φ), reduced scattering coefficient (μ'_s), and the tissue's actual refractive index n'.

Light absorbed by molecules and atoms can be used to generate thermal energy, emit fluorescence, or be used up in the reactions of the photochemical. The photon absorption probability per unit length of the medium is shown by the absorption coefficient. Absorption of light by a medium causes a decrease in brightness, which is described by the Beer-Lambert Law.

$$I = I_0 e^{-\mu_a x} \quad (1)$$

Here, I_o represents the incident light's intensity, μ_a is the absorption coefficient, x is the tissue's thickness. The scattering coefficient $\mu_s(\lambda)$ (cm^{-1}) describes a medium with multiple scattering particles and varying concentrations, which are expressed as a volume density (ρ_s) cm^3. The effectiveness of the scattering is proportional to the cross-sectional area of the particles. The scattering coefficient can be defined as follows:

$$\mu_s = \rho_s . \sigma_s \quad (2)$$

where, ρ_s defines the density of scattering particles per unit volume and σ_s defines the scattering cross-section. Equation (3) describes the density of scattering sites:

$$\rho_s = \frac{f_v}{V} \quad (3)$$

Here, f_v represents the concentration, and V represents the particle's volume. The equation for scattering cross-section (σ_s) is defined in (4):

$$\sigma_s = Q_s . A_s \quad (4)$$

where, Q_s is the fractional scattering efficiency and A_s is the real particle cross-section.

The reduced scattering coefficient (μ'_s) determines the decreased scattering coefficient and is used to represent the diffusion of photons in a random walk with step size $1/\mu'_s$:

$$\mu_s' = \mu_s(1 - g) \quad (5)$$

Here, g is the anisotropy, and can be calculated by finding the cosine of the scattering angle. Regarding the scattering phase function, its definition as the probability of scattering at different angles θ and ψ. These are the scattering angles in plane and perpendicular to scattering plane, respectively [15] (Fig. 2). An important metric for determining P(θ) is the scattering anisotropy factor g. It is defined as a parameter for computing the forwarding propagation retention following a single scattering event.

In this study, three monodisperse polystyrene aqueous solutions were used in the tests. An optical probe technique's sensitivity to light scattering from superficial tissues must be assessed using tissue phantoms. Using artificial tissues, preliminary findings from actual biological samples are presented. The ELSS method uses a different set of ingredients in its phantom recipe than do the other optical methods (DRS, FS, and RS). An aqueous suspension of monodisperse polystyrene with varying microsphere sizes makes up the majority of the optical phantom [6], [16]-[22]. The results of the

World Academy of Science, Engineering and Technology
International Journal of Biomedical and Biological Engineering
Vol:18, No:5, 2024

real malignant tissues' characterization may be predicted using variations in microsphere diameters. The optical properties (μ_s, g and μ'_s) of three different diameters of polystyrene suspension were shown in Fig. 3. In the region of 0.3 μm to 0.55 μm, this figure illustrates a considerable disparity in the values of μ_s for three particle sizes. Between 0.55 μm to 0.65 μm overlap was visible. There is a marginal distinction between the three particle sizes between 0.7 μm and 1 μm. For the short wavelength range of 0.3 μm to 0.5 μm, an overlap was demonstrated for the g value. However, a considerable variance in g over the range 0.5 μm and 1 μm. At μ'_s, it has been discovered a considerable variation in the range of 0.3 μm to 0.75 μm, while it found an overlap between 0.75 μm and 1 μm for 0.4 μm and 0.8 μm. However, the outcome does not vary noticeably for particles with a size of 2 μm.
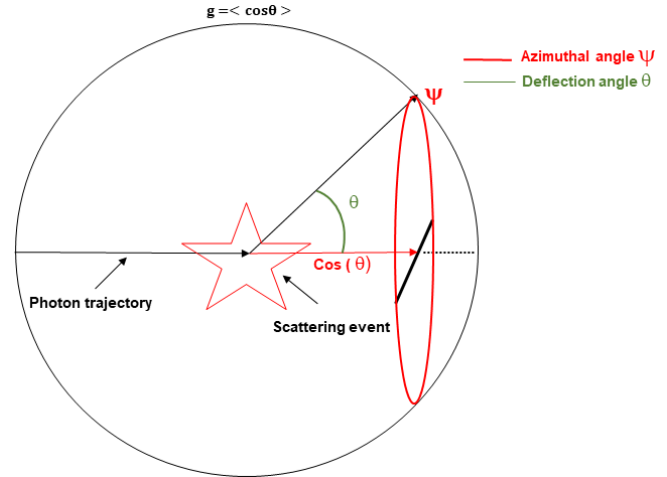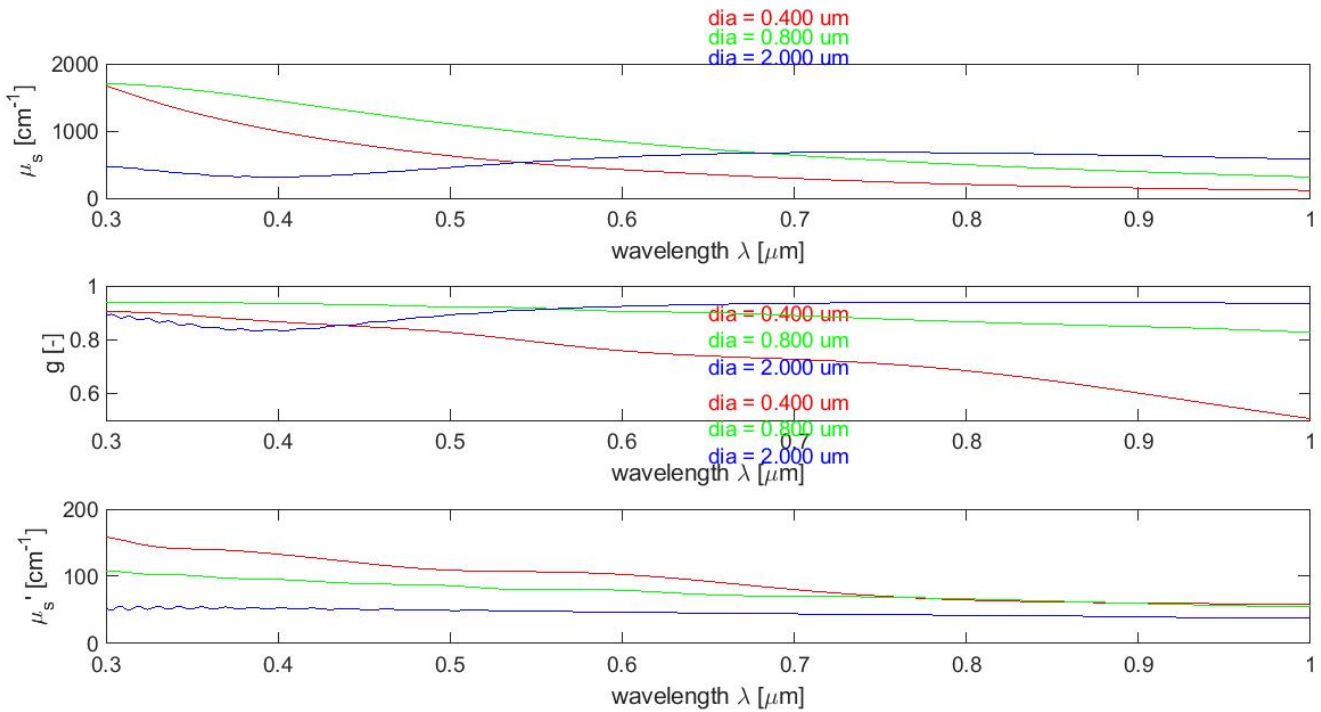

Fig. 2 Anisotropy in scattering

Fig. 3 The optical properties (μ_s, g and μ'_s) of PS particles with three different sizes, 2 μm, 0.8 μm, and 0.4 μm

In our experiments, scattering occurs near the Mie scattering transition. A size parameter X and the ratio of the refraction index (m) are primarily employed to classify the system. A size parameter X and the ratio of the refraction index (m) are primarily employed to classify the system. The proportion between the particle's spherical radius and the wavelength (photon's size) $\lambda = \lambda_o/n_m$ indicates the size parameter, which can be described as:

$$X = \frac{2\pi a n_m}{\lambda_0} \qquad (6)$$

Particle radius (a), light's initial wavelength (λ_0; 632.8 nm), and medium refractive index (n_m) are all input in (6). The ratio of the refractive index of the sphere (n_s) to that of the medium

that surrounds it (n_m) is defined in (7) (m):

$$m = \frac{n_s}{n_m} \qquad (7)$$

In this study, the refractive index for the polystyrene suspension was determined to be 1.58 [6] and it is 1.333 with regard to water. The total intensity of scattering light from a randomly polarized light source (S_{11}) determined in (8), which represents the scattering phase function $p(cos\theta)$.

$$p(cos\theta) = S_{11}(\theta) = \frac{|S_1(\theta)|^2 + |S_2(\theta)|^2}{2} \qquad (8)$$

$S_1(\theta)$ and $S_2(\theta)$ are the angular scattering functions, while

World Academy of Science, Engineering and Technology
International Journal of Biomedical and Biological Engineering
Vol:18, No:5, 2024

$P(\cos\theta)$ is the function that describes the scattering phase. As a result, we need S_1 and S_2 to compute S_{11}, which is equivalent to $p(\cos\theta)$ of the angular function. Accordingly, Henyey and Greenstein determined the plane wave components scattered at an angle [23]. The amplitude is expressed as a spherical function.

$$S_1(\theta) = \sum_{n=1}^{\infty} \frac{2n+1}{n(n+1)}(a_n\pi_n(\cos\theta) + b_n\tau_n(\cos(\theta))) \quad (9)$$

$$S_2(\theta) = \sum_{n=1}^{\infty} \frac{2n+1}{n(n+1)}(a_n\tau_n(\cos(\theta) + b_n\pi_n(\cos(\theta))) \quad (10)$$

π_n and τ_n are represented by Legendre Polynomials P_n

$$\pi_n(\cos(\theta)) = \frac{1}{\sin\theta}P_n(\cos(\theta)) \quad (11)$$

$$\tau_n(\cos(\theta)) = \frac{d}{d\theta}P_n(\cos(\theta)) \quad (12)$$

The Mie computation relies on two factors, a_n and b_n known as the Mie coefficients. Both are determined by analyzing the scattered field amplitudes.

$$a_n = \frac{\Psi'_n(y)\Psi_n(x) - m\Psi_n(y)\Psi'_n(x)}{\Psi'_n(y)\xi_n(x) - m\Psi_n(y)\xi'_n(x)} \quad (13)$$

$$b_n = \frac{m\Psi'_n(y)\Psi_n(x) - \Psi_n(y)\Psi'_n(x)}{m\Psi'_n(y)\xi_n(x) - \Psi_n(y)\xi'_n(x)} \quad (14)$$

Here, Ψ_n and ξ_n are the Riccati–Bessel functions.

II. MATERIALS AND METHODS

Initially, a mathematical model was developed to determine the optimal design parameters (fibres diameter and the separation between them). Then, in our lab, an appropriate optical probe configuration was fabricated. Following that, polystyrene spheres in suspension (PS) were used to create tissue phantom samples, and then varied PS dilutions of 2.5%, 1.25%, and 0.625% for three particle sizes of 2 μm, 0.8 μm, and 0.413 μm were used to achieve experimental results. The PS suspension was measured in the range of 450 nm to 1000 nm after being subjected to incident white light.

A. Mathematical Model

Equations in Mathematical Models

The Beer-Lambert rule and the typical Gaussian distribution function serve as the fundamental equations that describe our initial mathematical model. Gaussian beams of laser (light) are a common occurrence in optics. Gaussian distributions are used to simulate both the intensity profile of the light exiting the fibre and the overall amount of light gathered in the receiving fibre. A Gaussian beam's diameter is proportional to its full width at half maximum (FWHM) intensity.

$$f(X, \sigma, \mu) = \frac{1}{(2\pi\sigma^2)^{1/2}} e^{\frac{-(x-\mu^2)}{2\sigma^2}} \quad (15)$$

In this expression, x represents a positional variable, μ represents the fibre centre, and σ represents the FWHM. Other equations unique to the design are utilized in our research. The FWHM of the emerging beam along the z-axis (which is perpendicular to the face of the fibre aperture) is modelled by (16). Wider FWHM results from longer beam propagation. If this is also applied to the receiving fibre, the two beams will begin to overlap at a particular distance from the fibre face. This overlapping region is the sensing or interaction volume, and it is possible that light backscattered in this region will be captured by the receiving fibre (as shown in Fig. 4).
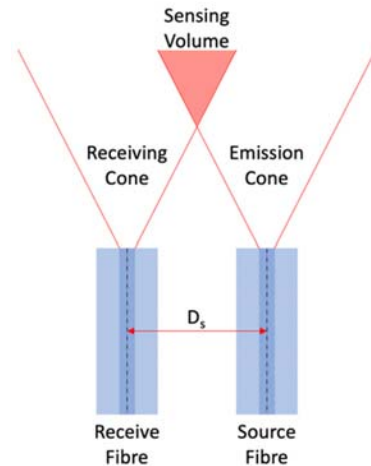

Fig. 4 Diagrammatic illustration showing how the sensing volume and the fibre separation Ds are produced by the overlap of the emission cones of the two fibres

Since most cancers begin in the epithelium (the outermost layer of cells), normal thickness is just 100 μm to 300 μm. Additionally, a crucial factor in detecting the top layer is the separation between the source fibre and the detector fibre. Consequently, the sensitivity will be much more limited to the epithelium if the space between the two fibres overlaps [15].
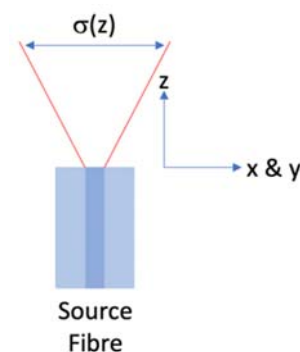

Fig. 5 Diagrammatic representation of the position dependent FWHM, σ as a function of distance from the fibre face

A three-dimensional spatial intensity distribution model in MATLAB was made by including the Gaussian intensity distribution for each fibre at discrete points forward of the fibre faces. This gave a straightforward way to quantify the coupling efficiency (intensity) for various fibre diameters, separations,

World Academy of Science, Engineering and Technology
International Journal of Biomedical and Biological Engineering
Vol:18, No:5, 2024

and refractive indices of the medium in front of the fibres for fibre core diameters specified by D_{core}. The full-width at half-maximum, or σ, is determined at various distances (z) from the fibre faces (Fig. 5 and (16)).

$$\sigma = \left(D_{core} + 2 * Y_{values(i)} * \tan(\theta_a)\right) \Big/ n\_\sigma$$

where, D_{core} is the diameter of the optical fibre core, θ_a is the acceptance angle and n_σ is a truncation parameter that governs the FWHM.

Fig. 6 illustrates how the NA and the material's refractive index affect the acceptable tangent angle.
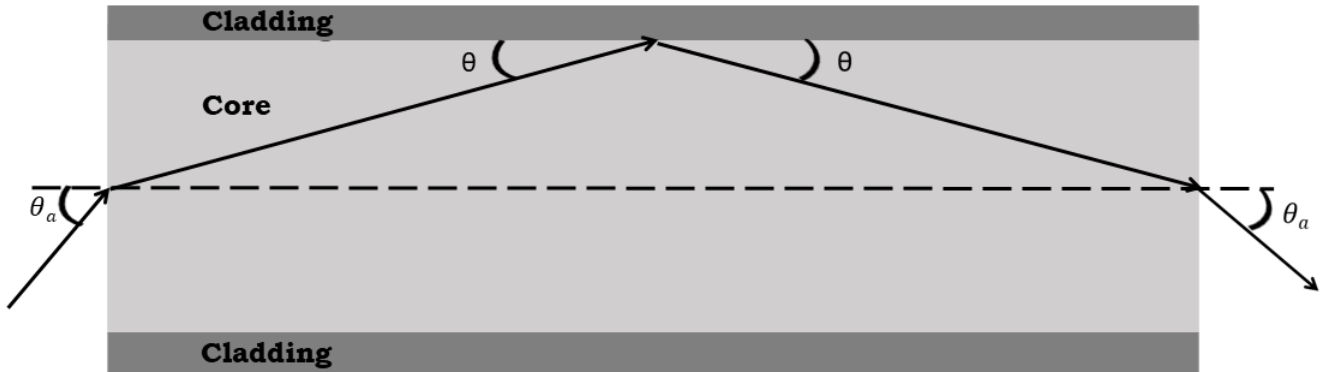
Fig. 6 The critical angle θ for total internal reflection depends on the acceptance angle θ_a and the effect of core diameter

The intensity of scattering in all three dimensions can be calculated with (17):

$$I(x,y,z) = e^{(-(\gamma*z))} * \left(1 \Big/ \sqrt{2*\pi*\sigma^2}\right) * \left[e^{-\frac{(y-\mu)^2}{2\sigma^2}} * \left(e^{-\frac{\left(x-\left(\mu-D_S/2\right)\right)^2}{2\sigma^2}} + e^{-\frac{\left(x+\left(\mu-D_S/2\right)\right)^2}{2\sigma^2}} \right) \right] \quad (17)$$

Here, μ is an arbitrary location between the centre of each fibre core in space (x, y). γ is the attenuation coefficient from the Beer-Lambert law and represents scattering and D_s is fibre separation.

Parameters Affecting the Mathematical Model

The Gaussian intensity function's extent must be reduced due to the finite width of optical fibre. The parameter n_σ is used simply to vary this truncation, as illustrated in Fig. 7. This figure demonstrated that the light does not reach 0 and ends abruptly at n-σ = 2. However, at n-σ = 6 illustrated that the light diminishing almost to zero at the periphery. Therefore, this parameter is used to determine the FWHM of the emerging beam and to provide variance relevant to the real fibres.

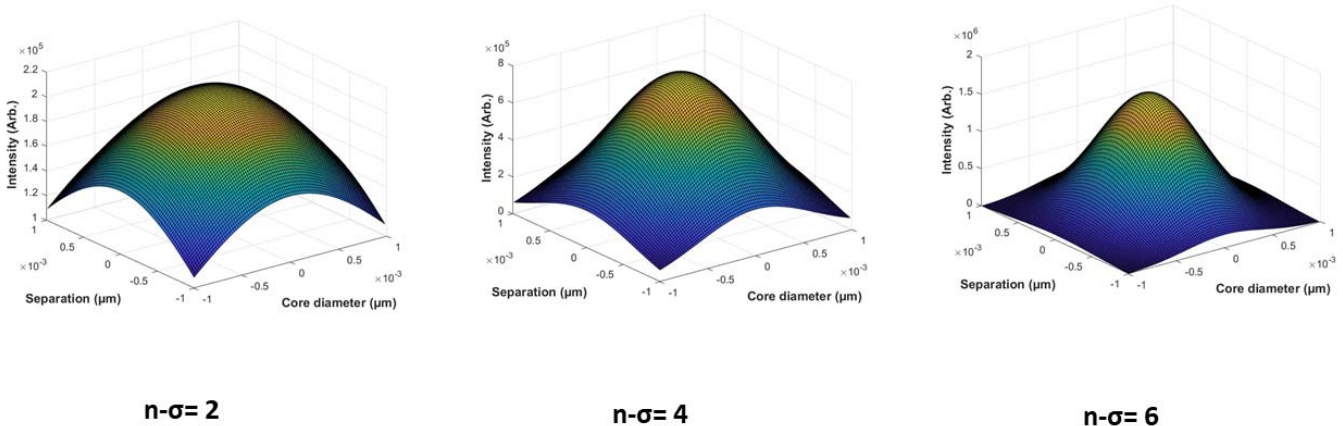n-σ= 2   n-σ= 4   n-σ= 6

Fig. 7 An illustration of the intensity profile for various sigma values (n-σ)

The acceptance angle (θ_a) plays an essential role in collecting incident light in optical fibres. It is defined as the maximum angle of a light ray that can enter the fibre. If the incident angle is at or below θ1, the beam will be propagated as shown in Fig. 8.

World Academy of Science, Engineering and Technology
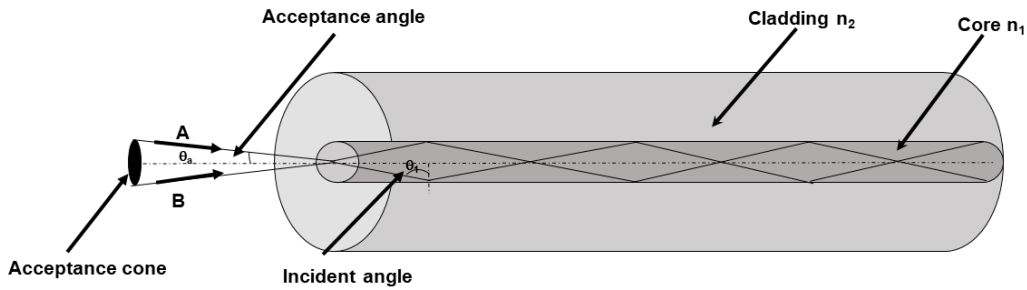International Journal of Biomedical and Biological Engineering
Vol:18, No:5, 2024

Fig. 8 The acceptance angle and the incident ray

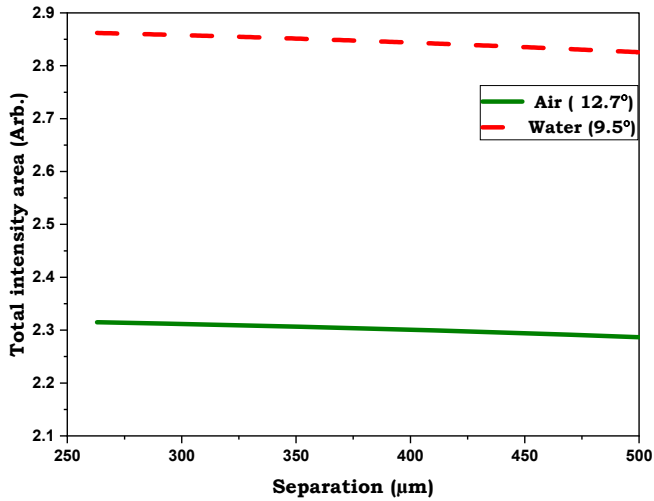

Fig. 9 Acceptance angle's impact on scattering intensity

When the value of θ1 decreases, this means the entire ray must be found within the acceptance cone to ensure total internal reflection occurs inside the fibre. The acceptance angle is typically reported in terms of numerical aperture (*NA*).

$$NA = n_0 \, sin\theta_a \qquad (18)$$

where n_0 is the ambient refractive index and θ_a is the acceptance angle.

From (18), *NA* is expressed a correlation between the ambient refractive index and the acceptance angle. *NA* plays an essential role in defining how light is collected from the source and retained light inside the fibre [24]. In our research, n_0, which is the refractive index of water, equals 1.333. The *NA* of our optical fibre is 0.22 therefore θ_a is 9.5°.

The Mathematical Method's Results

Fig. 9 illustrates the impact of the acceptance angle (θ_a water is 9.5° and θ_a air is 12.7°) on the scattering intensity with various separations. In general, the scattering intensity was found to be significantly higher at the water's acceptance angle than at the air's.
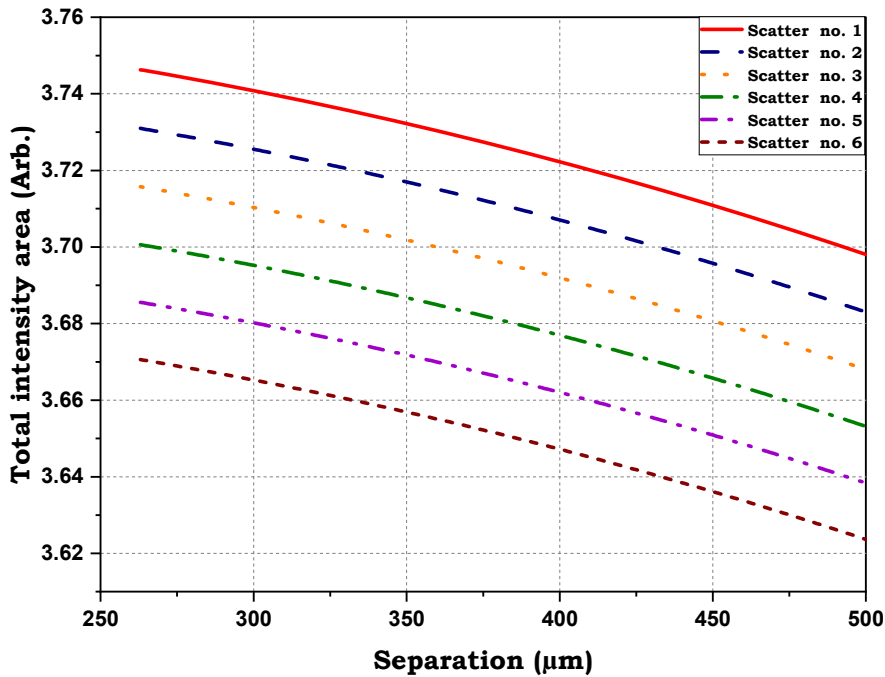

Fig. 10 The impact of scattering on separation

World Academy of Science, Engineering and Technology
International Journal of Biomedical and Biological Engineering
Vol:18, No:5, 2024

The refractive indices of the medium and the sphere, as well as the size of the particles, are independent factors in our study that fluctuate depending on the dependent variable (the scattering coefficient). The scattering coefficient is calculated theoretically based on the particle's cross section and the particle density per unit volume. As a result, we investigated how scattering affected our geometric model.

For fibre separations between 263 μm and 500 μm, the scattering effectiveness (scattering coefficient) is depicted in Fig. 10. Over the full range of fibre separation, a smaller scattering coefficient results in a higher scattering intensity. As shown in Fig. 10, the intensity of the scattered light substantially increases as the number of scattering events decreases.

Fig. 11 displays the scattering intensity as a function of fibre centre spacing. There was a general decrease in scattering with greater separation. Additionally, the scattering intensity is more effective in the design with a little spacing (263 μm) than it is in the design with a substantial separation (400 μm) (Fig. 11).
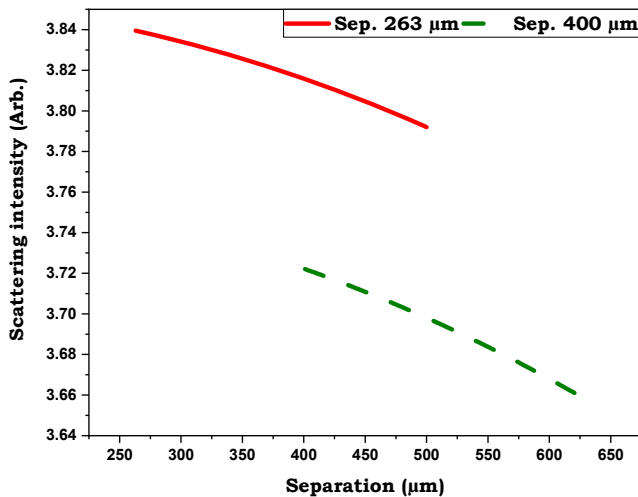

Fig. 11 Separation's impact on the intensity of the scattering

In Fig. 12, the influence of core diameter on scattering intensity is shown as a function of separation (from 120 to 500 μm). Over the whole separation range, scattering intensity was significantly higher for a 100 μm core diameter compared to a 200 μm core diameter (Fig. 12). These two diameters were chosen since they are important to the fabrication of our probe.

Intensity of coupling as a function of fibre separation at 15- and 25-degree acceptance angles is shown in Fig. 13. For two acceptance angles (15 and 25 degrees), the Lambertian emitter model shows how coupling intensity generally varies with distance between fibres. It stands to reason that the increased coupling efficiency will accompany the larger acceptance angle. The depth below the surface was extrapolated to derive the intensity seen here.

The analysis shown above is just meant to assess general patterns. Because the geometry of the fibre probe is mostly controlled by practical considerations, further investigation of this sort would be better suited to more complex commercial optical design tools.
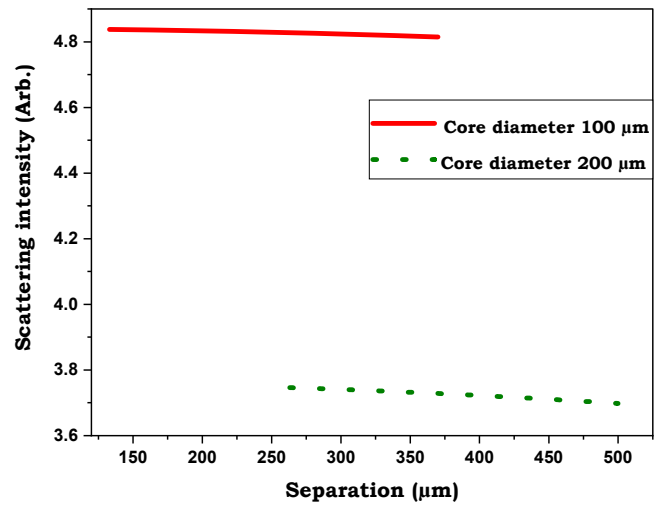

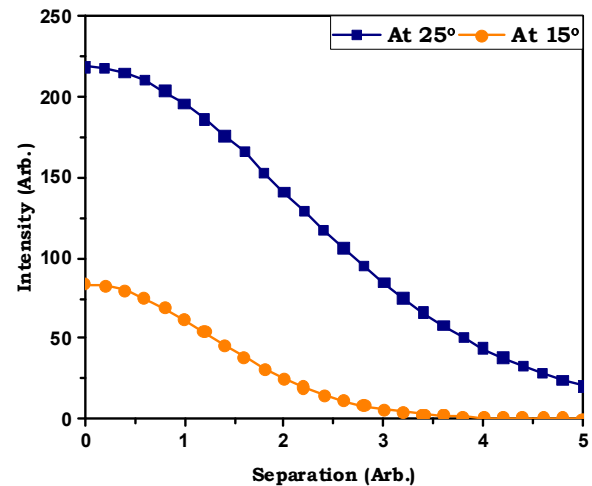Fig. 12 The diameter's impact on scattering intensity

Fig. 13 Coupling intensity at two different acceptance angles (15 and 25 degrees) as a function of fibre separation (Lambertian emitter model)

B. Method and Materials for the Experimental Part

Manufacturing and Geometric Design

Each of the two ELSS optical probes, 1 and 2, consists of two silica-silica identical fibres that are physically close to one another. One fiber is for illumination, and the other is for detection in the air, having a numerical aperture of 0.22. The 200 μm core diameter fibres are used in probe 1 and 100 μm diameter fibres are used in probe 2. For probe 1 and probe 2, the centre-to-centre distance is 263 μm and 132 μm, respectively. A sturdy stainless steel needle housing protects the distal end for safe handling. The overall assembly has dimensions of 0.8 and 0.5 mm, respectively. Figs. 14 and 15 demonstrated the design of the optical probe and its real physical manifestation.

Tissue Phantom Preparation

In the lab tests, three aqueous solutions of monodisperse

World Academy of Science, Engineering and Technology
International Journal of Biomedical and Biological Engineering
Vol:18, No:5, 2024

polystyrene microspheres (from Corpuscular Inc., Marvel of Nanoscience, and the USA) [25] were utilized. Diameters of the microspheres were 0.413 µm, 0.8 µm, and 2 µm. Samples of 250 microliters (µl) of stock (2.5%; the manufacturer's original concentration) and 250 µl of stock combined with 250 µl of deionized water (DI-W), with half of this combination serving as the first concentration (1.25%), respectively, were utilized. The remaining half is combined with 250 µl of DI-W to create a second concentration (0.625%) (Fig. 16). The ultimate concentration within various tissue types ranges from reduced scattering coefficient 12.972 cm^{-1} to 27.89 cm^{-1}. Reduced scattering coefficients for various tissue types range from 1.2 cm^{-1} to 40 cm^{-1} [6]. The reduction in scattering coefficients between 6.489 cm^{-1} and 111.584 cm^{-1} was used for all particle size measurements. Mie theory has been used to compute the reduced scattering coefficient at 632.8 nm using particle and DI-W refractive indices of 1.58 and 1.333, respectively. The Mie scattering is computed using the Scott Prahl calculator [26].

Instruments

The ELSS system comprised of an "Ocean Optics" Maya Pro USB Spectrometer and Original Equipment Manufacturer (OEM) ocean view software (Maya2000 Pro, Ocean Optics Company, US). This system uses a stabilized VIS-IR (Thorlabs Company, US) tungsten-halogen Light Source, with an optical resolution of 0.47 nm. The spectra are recorded and controlled by the computer. To fix the sample, an automated motor was employed. The probe was consistently inserted into the sample using a mobile scanning stage with an X-Y raster pattern. The stage's step size is under 1 µm (Fig. 17).
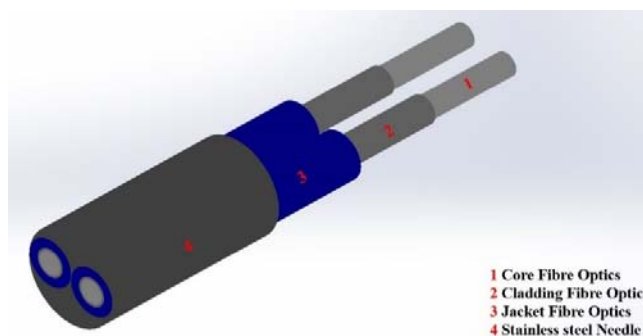

Fig. 14 The optical probe's design
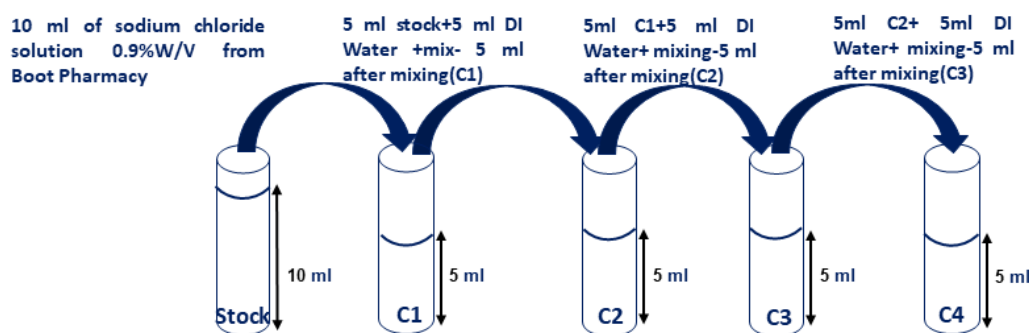

Fig. 15 The optical probe physically

Fig. 16 Preparation of polystyrene

Types of Configurations

Two identical optical fibres were joined within a 3D printed plastic housing for the first design. These two attached fibres are threaded into a stainless-steel needle for insertion into the sample. The source and reception fibres were equipped with SMA connections at the probe's other ends. The first configuration consists of two probes that have been made with various diameters (Fig. 18). These two probes will be compared in the result.

The goal here was to successfully detect isolated backscatter events. Lacking access to a fibre fusion splicer, it was not possible to produce a probe using a single fibre optic. To assure the detection of single backscattering, a second configuration was explored. A 400-µm-diameter core single-fibre probe has been constructed for this use. This probe has its two ends threaded into two independent stainless-steel needles. Sensing occurs at one end, while the other is butt-connected to two smaller-diameter fibres (probe 1, which consists of two identical fibres with core sizes of 200 m), partially overlapping, which will partially overlap and be bonded together using index-matching gel. This arrangement allows the illumination fibre to partially couple to the larger sensor fibre. Fig. 19 shows how light returning from the sensor fibre is partially linked into the spectrometer fibre.

Analysing Data

Equation (19) was used to adjust the obtained spectra for specular reflection and the wavelength dependency of the system's components [20].

$$R_{(\lambda)} = \frac{R(\lambda)_s - R(\lambda)_{bg}}{R(\lambda)_c - R(\lambda)_{bg}} \qquad (19)$$

World Academy of Science, Engineering and Technology
International Journal of Biomedical and Biological Engineering
Vol:18, No:5, 2024

Here, $R(\lambda)_s$ is the spectrum acquired by inserting a 5 mm probe into a suspension of monodisperse polystyrene microspheres. $R(\lambda)_{bg}$ is the background spectrum that was identified by defining the back reflection from a sample of pure water by inserting the tip of the optical probe into the DI-W's black container. $R(\lambda)_c$ is a spectralon spectrum (Labsphere, Inc., Ocean Optics). The spectral response of the system was calibrated using a reference spectrum taken from a spectrally flat diffuse reflector (Spectralon) that was placed about 1 mm above the probe.
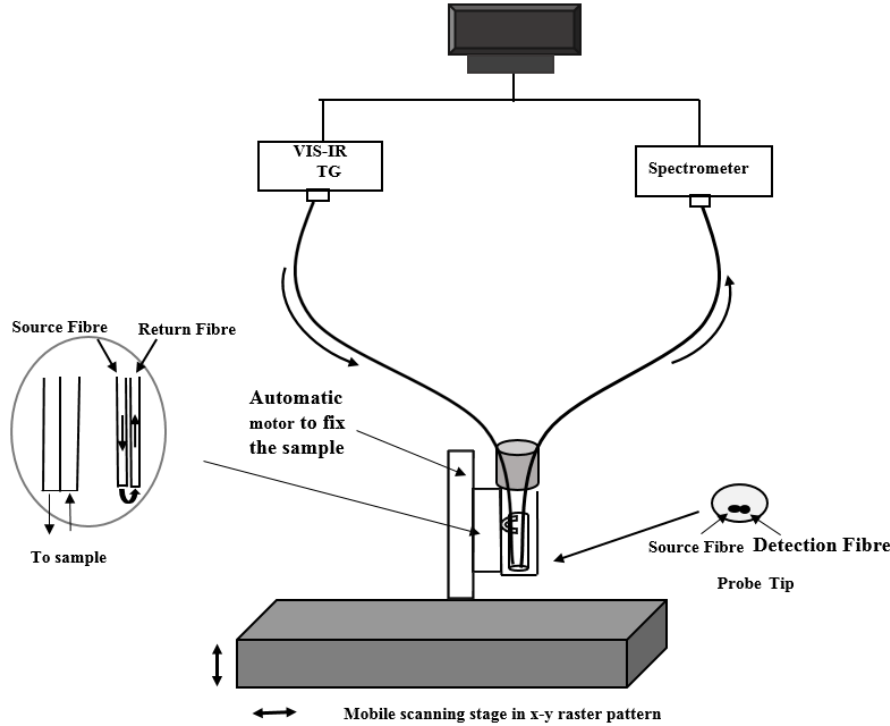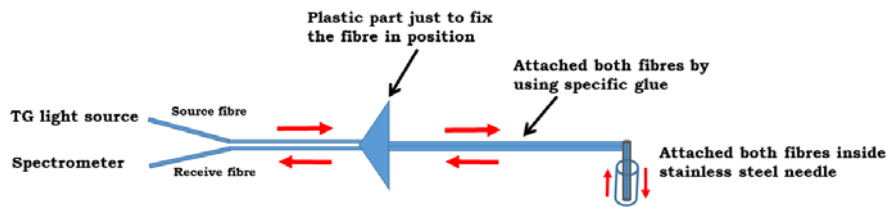

Fig. 17 The setup for the experiment

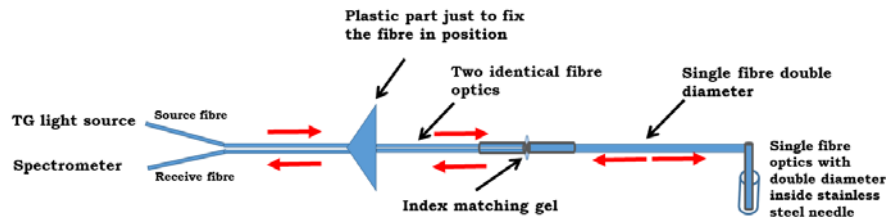Fig. 18 First setup's schematic diagram

Fig. 19 The second setup's schematic

III. RESULTS OF EXPERIMENTS

A. Effect of the Particle Size (Tissue Phantom Polystyrene Spheres in DI-W)

Fig. 20 displays the spectra for three polystyrene tissue phantoms with particle sizes of 2 μm, 0.8 μm, and 0.413 μm with a concentration of 0.625%. The reduced scattering coefficient ranges from 12.972 cm^{-1} and 27.89 cm^{-1} for this across a variety of tissue types. Fig. 22 demonstrates that over the whole range of wavelengths between 450 nm and 1000 nm, the number of peaks rises as particle size increases. The derivative (gradient) of the spectra is shown in Fig. 21. Oscillations in the derivative spectra increase in frequency with increasing particle size, even without the presence of the

World Academy of Science, Engineering and Technology
International Journal of Biomedical and Biological Engineering
Vol:18, No:5, 2024

background offset. Characteristic signatures for the various particle sizes are shown in Figs. 20 and 21 as spectra.
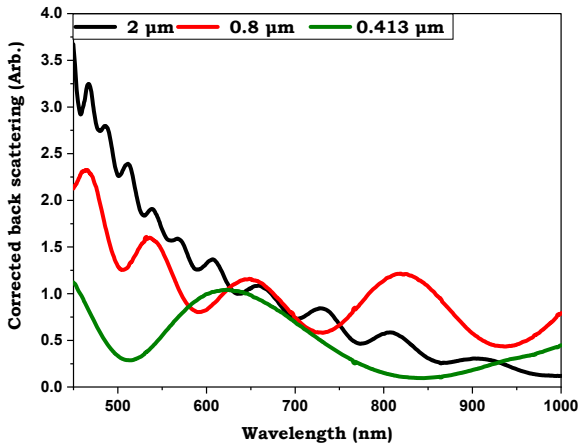

Fig. 20 Using an optical probe with a 100 μm diameter, three particle sizes with a concentration of 0.625% PS are compared. Each particle size has a unique signature
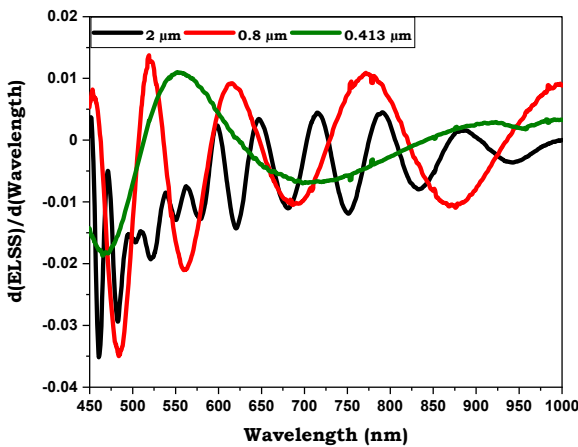

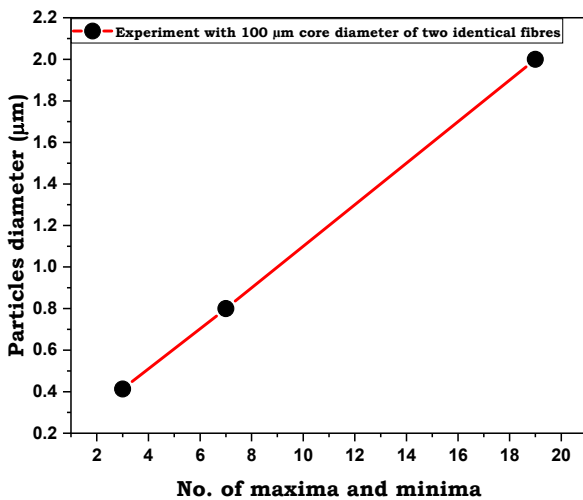Fig. 21 Derivatives of the spectra of Fig. 20

Fig. 22 The relationship between particle diameter and the total number of maxima and minima of the elastic scatter spectrum derivatives between 450 nm and 800 nm

Effect of the Core Diameter and the Separation Between Fibre Optics on Measurements of Phantoms of Non-Absorbing Tissue. Polystyrene in DI-W

Fig. 23 shows the spectra for three tissue phantoms at an initial concentration of 2.5%, with particle sizes of 2 μm, 0.8 μm, and 0.413 μm. It is clear from this figure that the signal intensity is higher for the 100 μm core diameter than the 200 μm fibre for each particle size. The fibre separations in this instance are 132 μm and 263 μm, respectively. The spectra in Fig. 24 were obtained with a 100 μm fibre core diameter from all particles with diverse concentrations (various reduced scattering coefficients). All particle spectra are evident in this figure at all concentrations, but 0.625% is particularly noticeable (Fig. 24 (c)).

Configuration of Spliced Fibre

To improve upon the inefficiency of the first setup, a second configuration was designed to maximize the likelihood of a successful scattering (single scattering) detection. Figs. 25-27 show a comparison between the signals obtained with the first probe structure (probe 1: side by side) and the second configuration (fibre splice). The initial PS concentration used in the experiment is 2.5% according to the manufacturer, and it is diluted by 1.25% and 0.625%. The probe is immersed in a polystyrene aqueous suspension of various particle sizes (2, 0.8, and 0.413 μm) in a black Eppendorf container. The maxima and minima in the second arrangement are less noticeable than they are in the first, as seen in Figs. 25-27. Since we wanted to recreate the setup that was described in [21], some obvious issues are present. Reduced fidelity in the signals acquired from the fibre splice configuration is largely due to poor coupling at the splice interface. There is a high probability that the source light will be reflected directly back to the spectrometer at the junction due to the imperfect fibre overlap.

The probe's design has a crucial role in determining the number of maxima and minima. The number of peaks and minima is influenced by particle size, as seen in Fig. 28. The number of maxima and minima in the derivative spectra often increases significantly as particle size increases, as demonstrated with all different probe designs. The number of maxima and minima is additionally altered by various designs and core diameters.

IV. DISCUSSION

The ideal fabrication measurements for an optical sensor system with applications in the diagnosis of cancer have been determined using a mathematical model. For sensing purposes, an artificial tissue composed of a polystyrene suspension of particles of different sizes has been developed and used. It is advisable to use a tissue phantom for testing the optical probe method's sensitivity to light scattering from superficial tissues. Synthetic tissues serve to illustrate preliminary biological specimen findings. In the mathematical model, it was discovered that the scattering intensity was substantially higher at the acceptance angle of the water than the air. In general, the coupling efficiency between the source and sensing fibres decreases as the refractive index fluctuations decrease.

World Academy of Science, Engineering and Technology
International Journal of Biomedical and Biological Engineering
Vol:18, No:5, 2024

Regarding the impact of scattering on our geometrical model, the scattering intensity increases when the number of scattering events drops significantly, which can be explained by the fact that inelastic scattering is the outcome of a photon's contact with a particle. In terms of fibre diameter, with a core diameter of 100 μm compared to 200 μm, the scattering intensity dramatically rises over the whole range of separation. This illustrates the two competing effects of increasing attenuation vs. increasing overlap. It is evident that coupling efficiency achieves its maximum at a particular distance from the fibre faces that serve as the "sensing volume."
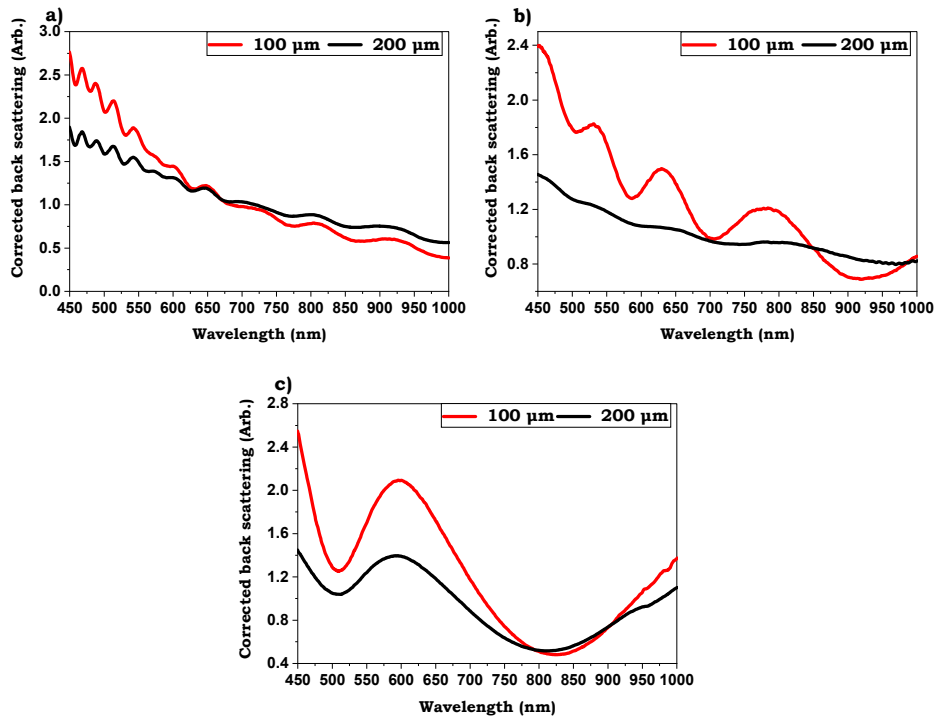

Fig. 23 Three particles with diameters of 2 μm, 0.8 μm, and 0.413 μm (a), (b), and (c) and a stock PS concentration of 2.5% were compared with respect to their 100 m and 200 μm cores diameters
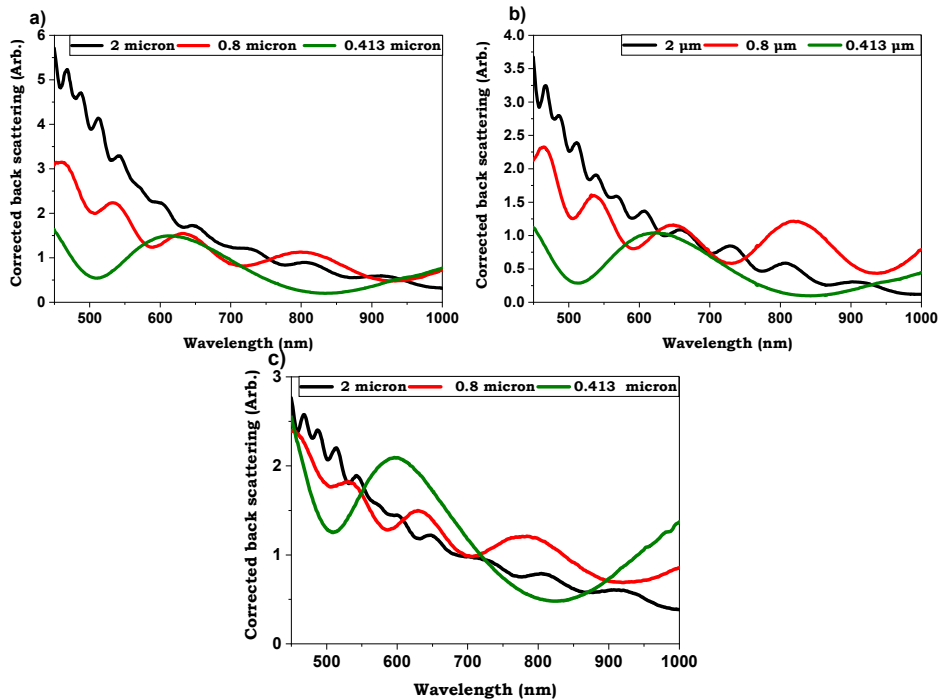

Fig. 24 The spectra of three particles with diameters of 2 μm, 0.8 μm, and 0.413 μm (a), (b), and (c) and PS concentrations of 2.5%, 1.25%, and 0.625%, respectively, as measured by a probe with a 100 μm core diameter

World Academy of Science, Engineering and Technology
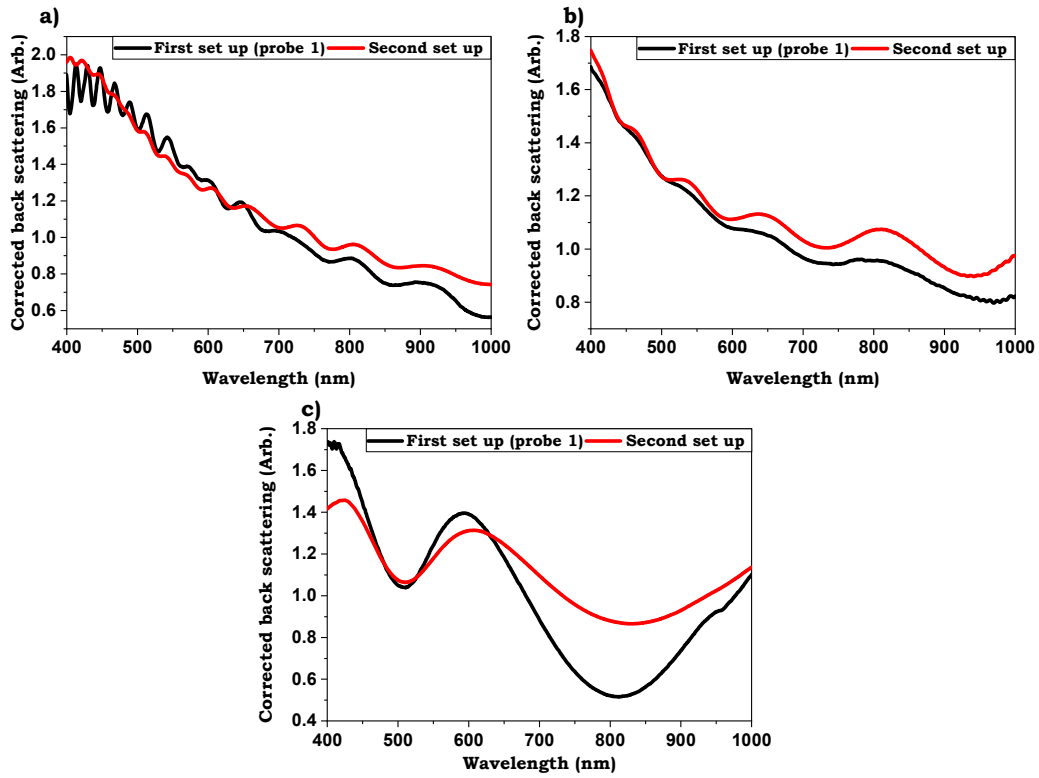International Journal of Biomedical and Biological Engineering
Vol:18, No:5, 2024

Fig. 25 The correlation between the first (Probe 1 with 200 μm for the two identical core diameter) and a second set up for three particles sizes 2 μm, 0.8 μm and 0.413 μm (a), (b), and (c) at 2.5% PS concentration

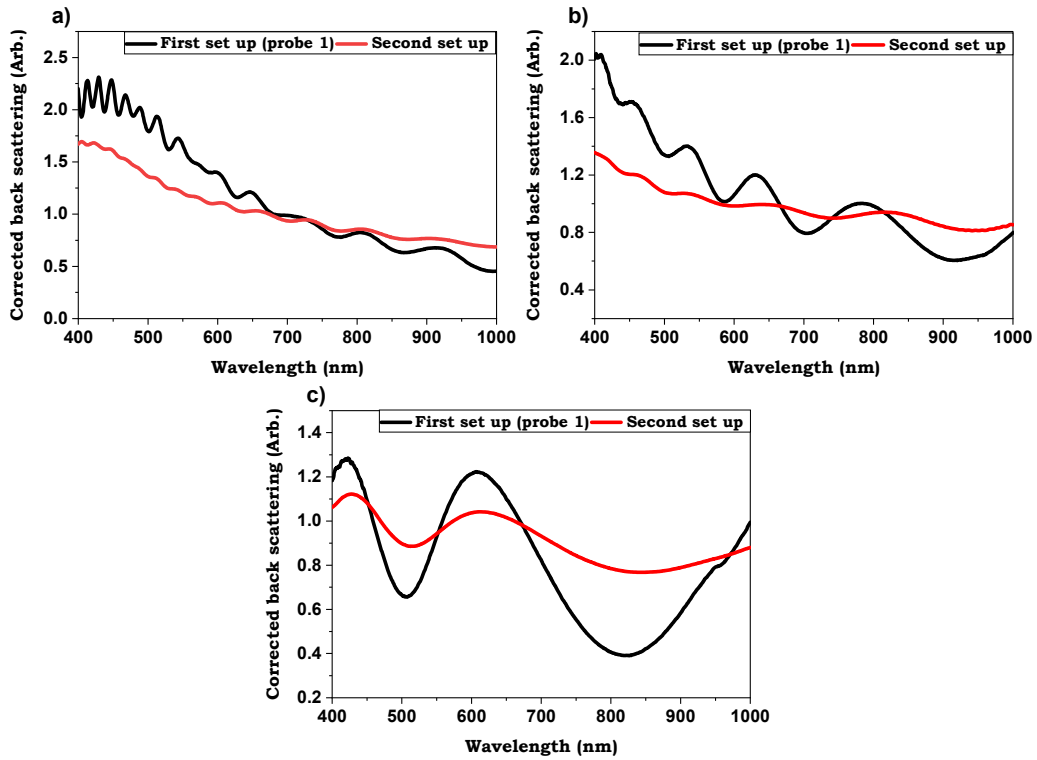

Fig. 26 The correlation between the first (Probe 1 with 200 μm for the two identical core diameter) and a second configuration set up for three particles sizes 2 μm, 0.8 μm and 0.413 μm (a), (b), and (c) at 1.25% PS concentration

World Academy of Science, Engineering and Technology
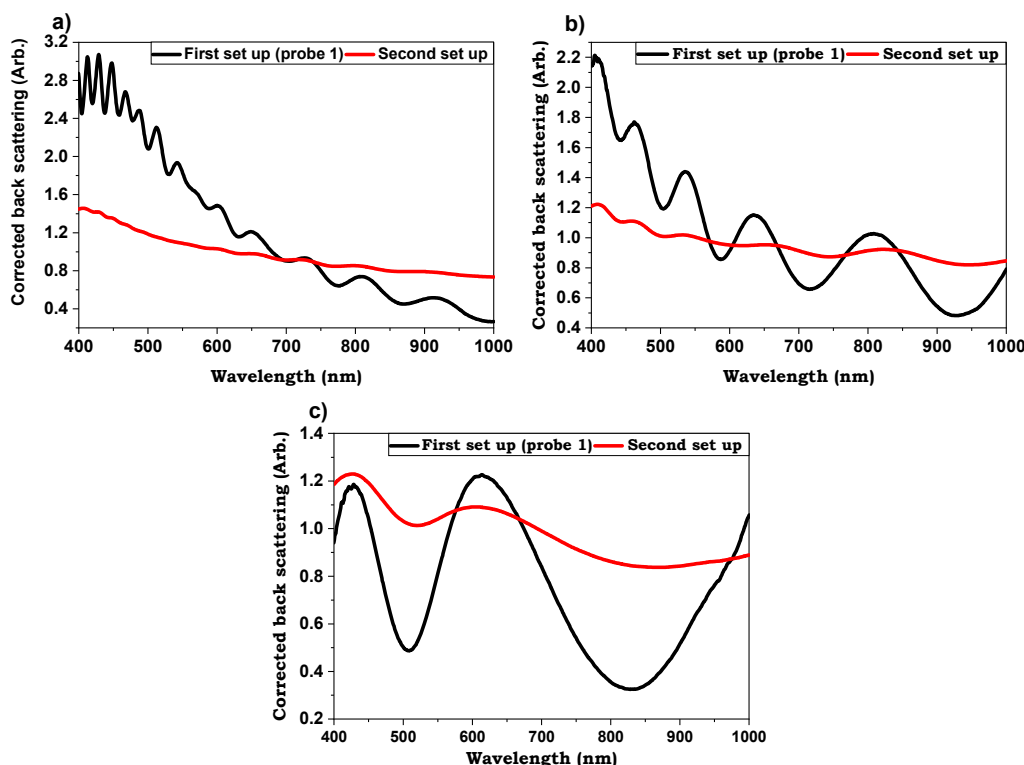International Journal of Biomedical and Biological Engineering
Vol:18, No:5, 2024

Fig. 27 The correlation between the first (Probe 1 with 200 μm for the two identical core diameter) and a second configuration set up for three particles sizes 2 μm, 0.8 μm and 0.413 μm (a), (b), and (c) at 0.625 % PS concentration
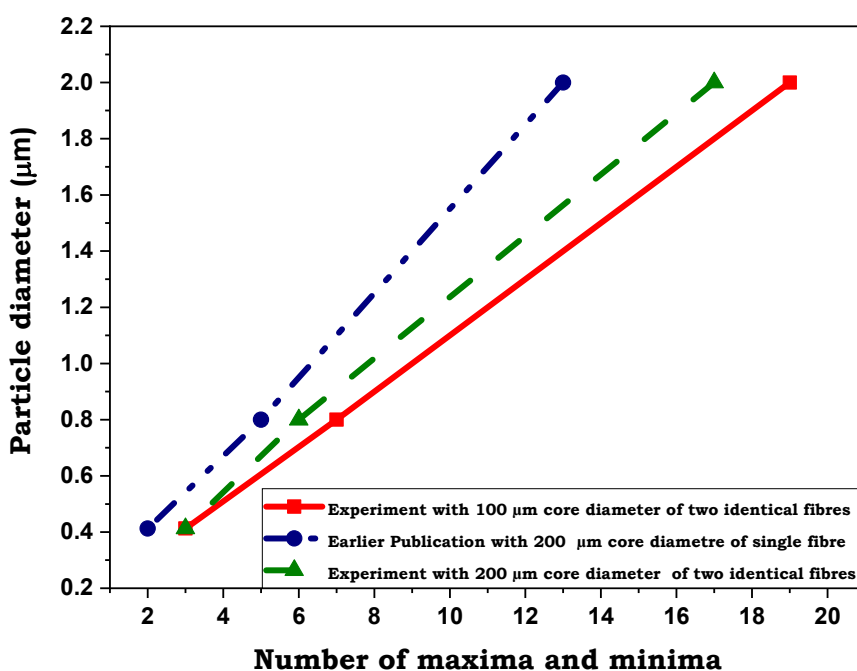

Fig. 28 Among three alternative designs, a number of maxima and minima

For various reasons, the separation of the fibre centres is crucial to the detection of tumours. The separation between the source and detector is one controlling factor for sampling the epithelium, which is the top layer and where most malignancies begin. The region that can be superficially investigated depends on how closely the source and detector are located to one another. The sensitivity is further constrained to the epithelium by the overlapping incident and detection fibres. The fact that the fibres are not physically close together poses the greatest challenge to our probe design. The geometrical probe's ability to detect high scatter angle events is increased by having the smallest distance between its illumination and light collection.

World Academy of Science, Engineering and Technology
International Journal of Biomedical and Biological Engineering
Vol:18, No:5, 2024

To be more precise, the scattering angle is zero for a photon that moves forward without scattering. The angle is high (180 degrees) if it is scattered backwards straight. The scattering angle must be relatively high—around 180 degrees—because our detection fibre is close to the source—in order for it to be possible to be detected. As a result, changing the source-detector separation will change the elastic scatter signal. According to the results of the mathematical model, it was shown that a smaller separation between the two designs (263 μm) is more effective in scattering intensity than a larger separation (400 μm).

The experimental detection portion of the detection process involved our manufacture optical sensor with different core diameters, 100 μm and 200 μm with 132 μm centre and 263 μm separation for detecting multi particle diameters of 0.413 μm, 0.8 μm, and 2 μm. There was a noticeable increase in scattering intensity over the whole range of separation with a core diameter of 100 μm compared to 200 μm. Despite the larger fibre's larger emission and collection regions, the smaller fibre's coupling is greater. On the other hand, the possibility of their coming closer together shows that separation predominates, and the smaller fibres produce a concentrated interaction volume.

The number of maxima and minima in the derivative spectra provided information on the diameter of the particles (Fig. 22). For particle diameters of 0.413 μm, 0.8 μm, and 2 μm, the total number of peaks (or minima) is essentially linearly linked to particle size. The ability to distinguish between healthy and cancerous cells depends critically on the size of the cells. Canpolat and Mourant confirmed this by calculating the scatterer size using the number of maxima and minima in the derivative spectra [21]. Here, the scattering medium is a monodisperse distribution of spherical objects with a known refractive index (1.58), operating over the range of 450-800 nm in wavelength [21]. This method is able to differentiate between scatterers of varying diameters (0.1 to 2 μm) [21]. Our study's probe can tell the difference between particles with diameters of 0.413 μm, 0.8 μm, and 2 μm by counting the number of maxima and minima in their spectra, which is directly proportional to the particle's size and the wavelength.

To sum up, there are two design factors that will have an impact on the effectiveness of scattering detection. The first of these is the centre-to-centre separation. Samples from the upper layer can be significantly improved by the short source-detector separation. This sensitivity will only affect the skin's epithelium, which is normally between 100 μm and 300 μm thick and where the majority of adult cancers develop [15]. In addition, because the lighting and collecting fibres are so near together, there can be only a small number of scattering events involving the collected light. The number of scattering events is diminished as the significance of factors such tissue size, shape, and refractive index increases [7]. The diameter of the optical fibre is the second factor that influences the scattering's quality. Single scatter events can be detected using optical fibres with small diameters. These photons provide information on the scattering's size [16]. Additionally, measuring particle size locally is made possible by probing a small volume [21]. Regarding the first design, a few restrictions are brought on by

the absorbance that could result from the separation of the two-fibre optics caused by the glue. This issue might reduce scattering effectiveness. Absorption in the medium decreases ELSS signals by a factor that varies with the collected photons' path length. Greater light absorption occurs along longer paths. A single fibre geometry, however, makes it possible to achieve a reduced path length.

V. CONCLUSION

At concentrations ranging from 2.5% to 0.625% (S to C2), the results showed that the optical probe with core diameters of 200 μm and 100 μm can distinguish between the PS particle sizes used in our research (2, 0.8, and 0.41 μm). Every size has a different signature. Additionally, the derivative spectrum changes as the size of the particle increases, resulting in a varied number of maxima and minima. The results also demonstrated that a 100 μm core diameter optical probe is superior to a 200 μm one. The second configuration type was an attempt to achieve single scattering events using the same single-fibre setup as in the paper's first configuration type [21]. On the other hand, if compared to the two identical optical probes that were located nearby, it had a lower resolution due to reflection at the fibre junction. Maxima and minima were more pronounced when using the twin fibre design.

REFERENCES

[1] G. A. Grillone *et al.*, "The color of cancer: Margin guidance for oral cancer resection using elastic scattering spectroscopy," (in Eng), *The Laryngoscope,* vol. 127 Suppl 4, pp. S1-s9, Sep 2017, doi: 10.1002/lary.26763.

[2] M. Turhan *et al.*, "Intraoperative assessment of laryngeal malignancy using elastic light single-scattering spectroscopy: A pilot study," (in Eng), *The Laryngoscope,* vol. 127, no. 3, pp. 611-615, Mar 2017, doi: 10.1002/lary.26224.

[3] G. C. Langhout *et al.*, "Differentiation of healthy and malignant tissue in colon cancer patients using optical spectroscopy: A tool for image-guided surgery," (in Eng), *Lasers in surgery and medicine,* Jul 20 2015, doi: 10.1002/lsm.22388.

[4] W. Jerjes, B. Swinson, D. Pickard, G. J. Thomas, and C. Hopper, "Detection of cervical intranodal metastasis in oral cancer using elastic scattering spectroscopy," (in Eng), *Oral oncology,* vol. 40, no. 7, pp. 673-8, Aug 2004, doi: 10.1016/j.oraloncology.2004.01.009.

[5] A. Sharwani *et al.*, "Assessment of oral premalignancy using elastic scattering spectroscopy," (in Eng), *Oral oncology,* vol. 42, no. 4, pp. 343-9, Apr 2006, doi: 10.1016/j.oraloncology.2005.08.008.

[6] A. Sircan-Kucuksayan, T. Denkceken, and M. Canpolat, "Differentiating cancerous tissues from noncancerous tissues using single-fiber reflectance spectroscopy with different fiber diameters," (in Eng), *Journal of biomedical optics,* vol. 20, no. 11, p. 115007, Nov 2015, doi: 10.1117/1.jbo.20.11.115007.

[7] A. H. Hielscher, Mourant, J.R. AND Bigio, J. I., "Biomedical Diagnostics with Elastic Light Scattering in Cell Suspensions and Tissues " *19th International Conference* 1997.

[8] T. Upile, W. Jerjes, H. Radhi, J. Mahil, A. Rao, and C. Hopper, "Elastic scattering spectroscopy in assessing skin lesions: an "in vivo" study," (in Eng), *Photodiagnosis and photodynamic therapy,* vol. 9, no. 2, pp. 132-41, Jun 2012, doi: 10.1016/j.pdpdt.2011.12.003.

[9] E. Omar, "Current concepts and future of noninvasive procedures for diagnosing oral squamous cell carcinoma--a systematic review," (in Eng), *Head & face medicine,* vol. 11, p. 6, 2015, doi: 10.1186/s13005-015-0063-z.

[10] H.-J. Wei, J.-J. L. Da Xing, H.-M. Gu, G.-Y. Wu, and Y. Jin, "Determination of optical properties of normal and adenomatous human colon tissues in vitro using integrating sphere techniques," *World Journal of Gastroenterology: WJG,* vol. 11, no. 16, p. 2413, 2005.

[11] V. Dremin *et al.*, "Imaging of early stage breast cancer with circularly

World Academy of Science, Engineering and Technology
International Journal of Biomedical and Biological Engineering
Vol:18, No:5, 2024

polarized light," in *Tissue Optics and Photonics*, 2020, vol. 11363: International Society for Optics and Photonics, p. 1136304.

[12] I. H. Aboughaleb, M. H. Aref, and Y. H. El-Sharkawy, "Hyperspectral imaging for diagnosis and detection of ex-vivo breast cancer," *Photodiagnosis and photodynamic therapy,* vol. 31, p. 101922, 2020.

[13] J. Robijns, S. Censabella, P. Bulens, A. Maes, and J. Mebis, "The use of low-level light therapy in supportive care for patients with breast cancer: review of the literature," *Lasers in medical science,* vol. 32, no. 1, pp. 229-242, 2017.

[14] X. Xu, H. Lu, and R. Lee, "Near infrared light triggered photo/immuno-therapy toward cancers," *Frontiers in Bioengineering and Biotechnology,* vol. 8, 2020.

[15] T. Vo-Dinh, *Biomedical_Photonics_Handbook*. USA, 2003.

[16] M. Baykara, T. Denkceken, I. Bassorgun, Y. Akin, S. Yucel, and M. Canpolat, "Detecting positive surgical margins using single optical fiber probe during radical prostatectomy: a pilot study," (in Eng), *Urology,* vol. 83, no. 6, pp. 1438-42, Jun 2014, doi: 10.1016/j.urology.2014.02.020.

[17] T. Denkceken *et al.*, "Elastic light single-scattering spectroscopy for the detection of cervical precancerous ex vivo," (in Eng), *IEEE transactions on bio-medical engineering,* vol. 60, no. 1, pp. 123-7, Jan 2013, doi: 10.1109/tbme.2012.2225429.

[18] T. Denkceken, M. Canpolat, M. Baykara, I. Bassorgun, and A. Aktas-Samur, "Diagnosis of pelvic lymph node metastasis in prostate cancer using single optical fiber probe," (in Eng), *International journal of biological macromolecules,* Oct 23 2015, doi: 10.1016/j.ijbiomac.2015.10.062.

[19] M. Canpolat, A. Akman-Karakas, G. A. Gokhan-Ocak, I. C. Bassorgun, M. Akif Ciftcioglu, and E. Alpsoy, "Diagnosis and demarcation of skin malignancy using elastic light single-scattering spectroscopy: a pilot study," (in Eng), *Dermatologic surgery: official publication for American Society for Dermatologic Surgery [et al.],* vol. 38, no. 2, pp. 215-23, Feb 2012, doi: 10.1111/j.1524-4725.2011.02174.x.

[20] M. Canpolat, M. Akyuz, G. A. Gokhan, and R. Tuncer, "Intra-operative brain tumer detection using elastic light single scattering spectroscopy: a feasibility study.," *Journal of biomediacl optics* vol. 14, no. 5, pp. 054021-1- 054021-7, 2009.

[21] M. Canpolat and J. R. Mourant, "Particle size analysis of turbid media with a single optical fiber in contact with the medium to deliver and detect white light," (in Eng), *Applied optics,* vol. 40, no. 22, pp. 3792-9, Aug 1 2001.

[22] A. Amelink, M. P. Bard, S. A. Burgers, and H. J. Sterenborg, "Single-scattering spectroscopy for the endoscopic analysis of particle size in superficial layers of turbid media," (in Eng), *Applied optics,* vol. 42, no. 19, pp. 4095-101, Jul 1 2003.

[23] L. G. Henyey and J. L. Greenstein, "Diffuse radiation in the galaxy," *The Astrophysical Journal,* vol. 93, pp. 70-83, 1941.

[24] L. C. Chin, W. M. Whelan, and I. A. Vitkin, "Optical fiber sensors for biomedical applications," in *Optical-thermal response of laser-irradiated tissue*: Springer, 2010, pp. 661-712.

[25] Microspheres-Nanospheres. "Plain polystyrene nanospheres and microspheres." https://www.microspheres-nanospheres.com/Microspheres/Organic/Polystyrene/PS%20Plain.htm accessed 2021, March 11.

[26] Scott Prahl. "Mie scattering calculations." https://omlc.org/calc/mie_calc.html accessed 2021, March 11.